9

Original article

Haiyan Yin*, Maziar Sedighi Moghaddam, Mikko Tuominen, Andra Dėdinaitė, Magnus Wålinder and Agne Swerin*

Non-fluorine surface modification of acetylated birch for improved water repellence

https://doi.org/10.1515/hf-2020-0236 Received November 11, 2020; accepted February 12, 2021; published online April 5, 2021

Abstract: In this work, a non-fluorinated surface treatment, i.e., hydrophobized silicone nanofilaments, was applied on both birch and acetylated birch wood samples via a gas-phase based reaction. A superhydrophobic behavior was observed on both the surface-modified samples as revealed by the static water contact angles (CAs) greater than 160°, also valid for samples prepared with the shortest reaction time of 1 h. The dynamic wettability behavior of the samples was studied by a multicycle Wilhelmy plate method. The surface-modified acetylated birch exhibited a pronounced enhanced water resistance, resulting in very low water uptake of 3 ± 1 wt% after 100 cycles, which was not only about 29 and 5 times lower than

that of the non-surface-modified birch and acetylated birch, respectively, but also three times lower than that of the surface-modified birch. Moreover, the aesthetic appearance of the acetylated wood was maintained as the surface modification only resulted in a small color change. This work shows the potential of preparing super water-repellent wood by non-fluorinated surface modification.

Keywords: acetylated wood; multicycle Wilhelmy plate method; non-fluorine surface modification; silicone nanofilaments; superhydrophobic coating.

1 Introduction

Owing to its renewability and sustainable forestry, wood is today the most abundant and low-carbon emitting material for large scale uses in the construction and furniture industries. Due to its hydrophilic nature, wood-based products are, however, susceptible to dimensional deformation and biological degradation, especially in outdoor applications. Improving the water-resistance of wood-based products has therefore gained increased attention in recent years (Cademartori et al. 2017; Hill 2006; Källbom et al. 2018; Meyer-Veltrup et al. 2017).

Bulk modification of wood is one common approach for improving the water repellence of wood-based products. The bulk modification lowers the hygroscopicity of wood by altering the properties of wood cell walls. Typical bulk modification methods include thermal modification and chemical modifications using various chemicals (Herrera et al. 2018; Hill 2006; Källbom et al. 2020; Rowell 2007). One of the commonly used chemical treatments is acetylation, in which the accessible hydroxyl groups in the wood cell-wall react with acetic anhydride and form ester bonds (Rowell et al. 1994). It was reported that the equilibrium moisture content of acetylated pine was reduced to 8.4% at 90% RH, which was 2.6 times lower than that of non-acetylated pine (Rowell 2014). Apart from the increased moisture resistance, the acetylated wood showed improved physical, mechanical and biological

and Architectural Engineering, School of Architecture and the Built

Sweden

Environment, KTH Royal Institute of Technology, SE-10044 Stockholm,

^{*}Corresponding authors: Haiyan Yin, Material and Surface Design, Division Bioeconomy and Health, RISE Research Institutes of Sweden, Box 5607, SE-11486 Stockholm, Sweden; and Division of Building Materials, Department of Civil and Architectural Engineering, School of Architecture and the Built Environment, KTH Royal Institute of Technology, SE-10044 Stockholm, Sweden, E-mail: haivanvi@kth.se: and Agne Swerin, Division of Surface and Corrosion Science, Department of Chemistry, School of Engineering Sciences in Chemistry, Biotechnology and Health, KTH Royal Institute of Technology, SE-10044 Stockholm, Sweden; and Chemical Engineering, Department of Engineering and Chemical Sciences, Faculty of Health, Science and Technology, Karlstad University, SE-65188 Karlstad, Sweden, E-mail: agne.swerin@kau.se Maziar Sedighi Moghaddam and Mikko Tuominen, Material and Surface Design, Division Bioeconomy and Health, RISE Research Institutes of Sweden, Box 5607, SE-11486 Stockholm, Sweden Andra Dedinaite, Chemical Process and Pharmaceutical Development, Division Bioeconomy and Health, RISE Research Institutes of Sweden, Box 5607, SE-11486 Stockholm, Sweden; and Division of Surface and Corrosion Science, Department of Chemistry, School of Engineering Sciences in Chemistry, Biotechnology and Health, KTH Royal Institute of Technology, SE-10044 Stockholm, Sweden Magnus Wålinder, Division of Building Materials, Department of Civil

properties (Bongers and Uphill 2019; Chai et al. 2017). Moreover, the acetylation process can be defined as a nontoxic chemical treatment. Therefore, there has been a growing interest in using acetylated wood for improving the performance of wood in recent years (Beck et al. 2018; Hansmann et al. 2004; Hung et al. 2016; Joffre et al. 2017; Laine et al. 2016; Ringman et al. 2020). However, studies showed that acetylation of wood only increased the apparent water contact angle (CA) to a minor extent, e.g., from 69° to 83° (Bryne and Wålinder 2010), which suggests that the wood is still prone to interaction with moisture, thus increasing the risk e.g., for surface discoloration and mold growth.

Another approach is to modify wood surfaces by a superhydrophobic layer. Superhydrophobic surfaces, inspired by the lotus leaf structure, show non-wettability and good self-cleaning properties when in contact with water. A superhydrophobic layer on wood can be achieved by combining a nanoscale structure with low surface energy chemistry on top (Teisala and Butt 2018; Tuteja et al. 2011; Wang et al. 2020). Usually, nanoparticles such as SiO₂, ZnO, and TiO₂ are used to create the nanoscale roughness on wood surfaces (Gao et al. 2015; Guo et al. 2017; Pandit et al. 2020; Sedighi Moghaddam et al. 2016a; Tuominen et al. 2016). For example, Pandit et al. (2020) reported a superhydrophobic coating on wood prepared by TiO₂ nanoparticles and perfluorooctyltriethoxysilane. The modified wood exhibited excellent repellence towards water and liquids with lower surface tension. Yin et al. (2020) reported that fluorinated silicone nanofilaments layers could improve the liquid repellence of wood surfaces, leading to high static CAs and low liquid uptake rate and level towards water, ethylene glycol and hexadecane. Silicone nanofilaments layer is a promising surface modification method for improving the water-resistance of wood by ultra/superhydrophobization via micro- and nano-scale surface roughness of wood and low surface energy chemistry. Moreover, no extra reagents are involved in the gasphase based reaction, thus reducing possible negative effects to the environment during the modification process.

A superhydrophobic surface is not a barrier for vapor from diffusing through an air layer into a hygroscopic substrate (Swerin and Wåhlander 2009; Yin et al. 2020). Therefore, even though superhydrophobic surfaces repel water, the final liquid uptake of the surface-modified wood can still be high as a result of liquid diffusion, and plausibly solubility, into the hygroscopic substrate. This effect shows that the application of a superhydrophobic coating to improve the liquid repellence of wood is still limited.

A superhydrophobic layer improves the water repellence of wood surfaces; acetylation, on the other hand,

reduces the number of the hydroxyl groups in the wood substance, thus reducing its affinity for water sorption. This encouraged the current study whether such a combination, i.e., applying a superhydrophobic layer on the acetylated wood, can lead to a significantly enhanced liquid resistance of wood. To our knowledge, no previous work has investigated this combination of bulk and surface modification.

In this work, the silicone nanofilaments were applied on acetylated wood surfaces through a gas-phase based silicone nanofilaments preparation method at reduced pressure. To reduce the potential hazard to environmental and human health, a non-fluorinated alkylsilane is utilized in the following hydrophobization process. Apart from the static CA measurement, the dynamic wettability of the surface-modified wood was studied by a multicycle Wilhelmy plate method. This work shows the possibility of achieving extremely low water uptake of wood using a nonfluorinated surface modification approach.

2 Materials and methods

2.1 Materials

The birch veneers were provided by Koskisen Oy in Finland. Half of the received birch veneers were acetylated by Accsys in Arnhem, the Netherlands, according to the process described on their webpage (ACCSYS 2020). According to Accsys, the acetyl content of the acetylated birch veneers was above 20%. The dimensions of the birch and acetylated birch wood samples used in this work were in approximately $30 \times 20 \times 1 \text{ mm}^3$ in the longitudinal, tangential and radial directions (L \times T \times R), respectively. The average moisture content was 5 and 1.4%, respectively, for the birch and acetylated birch.

2.2 Wood surface modification

The birch and acetylated birch wood samples were first surfacemodified by silicone nanofilaments at reduced pressure. The schematic illustration of the reaction setup for preparing silicone nanofilaments is shown in Figure 1a. Specifically, the wood samples (a total surface area of around 70 cm² for each type) were placed together with a vial containing 300 µL of trichloromethylsilane (TCMS, 99%, Sigma-Aldrich) and a vial containing 75 μL of water (Type 1, Milli-Q) in a sealed desiccator (reaction chamber, ca 5.7 L), which was connected to a rotary vane vacuum pump (Edwards). The reaction chamber was evacuated to the pressure of 5 kPa before the reaction started. The samples with a reaction time of 1, 2, 5 and 20 h were prepared. Figure 1b shows the RH change in the reaction chamber, which was measured by placing a hygrometer (Testo 174) together with the water in the chamber. The moisture absorption capacity for acetylated birch wood and birch wood is different. Therefore, to ensure the same RH changes in the synthesis of silicone nanofilaments, acetylated and non-acetylated wood samples were placed in the chamber together.

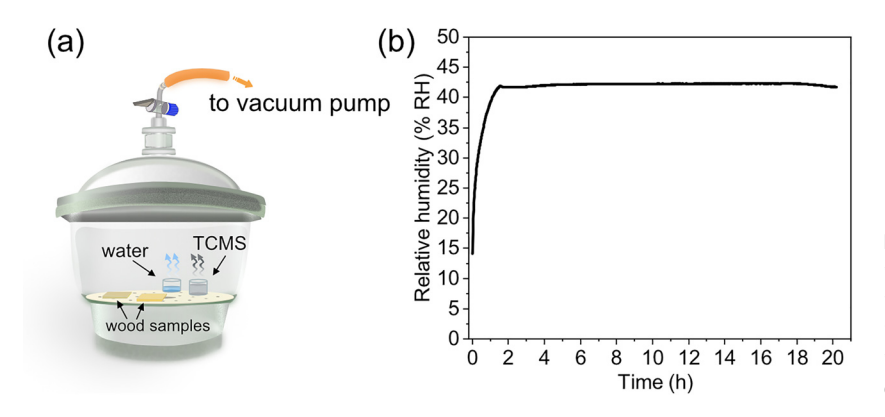


Figure 1: (a) Schematic illustration of the reaction setup for preparing silicone nanofilaments in gas phase at a reduced pressure of 5 kPa, (b) the corresponding relative humidity versus time in the reaction chamber with wood samples.

To further reduce the surface energy, the silicone nanofilaments coated samples were hydrophobized by chemical vapor deposition of trichloro(octyl)silane (TCOS, 97%, Sigma-Aldrich) for 2 h in a second step. Prior to the second step, the samples were plasma-activated in an 18 W air plasma cleaner (PDC-3XG, Harrick) for 5 min. In this process, the hydrophobic methyl groups of the silicone nanofilaments on the surfaces were converted into hydrophilic hydroxyl groups, which facilitated the bonding of TCOS molecules on the surface in the second step. The surface-modified birch and acetylated birch samples are denoted SMB and SMAB, respectively.

2.3 Characterization

Scanning electron microscopy (SEM) (FEI Quanta FEG 250) was utilized for imaging of the wood surfaces. The SEM characterization was performed at an accelerating voltage of 10 kV with a working distance of 10 mm in a low vacuum mode (LV-SEM) of 7 kPa. No surface pre-coating was applied. The diameter distribution of the silicone nanofilaments was calculated by analyzing the SEM images of the SMB and SMAB wood using ImageJ software. At least 1000 nanofilaments were chosen in the calculation for each sample. Fourier-transform infrared spectroscopy (FTIR) (Spectrum One, Perkin Elmer) equipped with an attenuated total reflection was used to study the chemical compositions on the wood surfaces. All spectra were recorded between 4000 and 400 cm⁻¹ at a resolution of 4 cm⁻¹ and 16 scans per sample.

The color of the wood samples was measured using an optical spectrophotometer X-Rite SP60 D65/10° illumination. The CIE LAB color space coordinate system was used to evaluate the color changes of the wood samples after the surface modification. Three parameters, viz., L^* , a^* , and b^* were recorded, where L^* represents lightness $(L^* = 100 \text{ for pure white}, L^* = 0 \text{ for total blackness}); +a^* \text{ represents}$ redness while $-a^*$ for green; $+b^*$ represents yellowness while $-b^*$ for blue. The total color change (ΔE^{\star}) was calculated according to the equation:

$$\Delta E^* = \sqrt{\Delta L^{*2} + \Delta a^{*2} + \Delta b^{*2}} \tag{1}$$

where ΔL^* , Δa^* , and Δb^* are the differences between the color of the wood samples before and after the surface modification. At least eight spots were analyzed for each sample.

The wettability of the wood and surface-modified wood was studied using an optical CA goniometer (OCA40, DataPhysics) equipped with a high-speed CCD camera (max 2200 images s⁻¹).

Measurements were performed in a climate-controlled room of $50 \pm 3\%$ RH at 23 ± 1 °C. A water drop of 10 µL was chosen as the surface-modified wood was superhydrophobic and drops of a smaller volume could not be dispensed on the surfaces. The tilting speed of the roll-off angle measurement was 1.58° s⁻¹. The static CAs and roll-off angles (ROAs) of water (Type 1, Milli-Q, surface tension 72.3 \pm 0.2 mN m⁻¹) were determined by the SCA 20 (DataPhysics) software using Young-Laplace fitting. At least 10 droplets were analyzed in each case.

A Sigma 70 tensiometer from KSV Instruments (now Biolin Scientific) was used for measuring the wetting properties and water uptake of the unmodified and surface-modified wood samples. The measurements followed a previously developed method (Sedighi Moghaddam et al. 2013, 2016b). Specifically, a 100-cycle Wilhelmy plate measurement was performed with the wood veneer in water. The immersion and withdrawal velocity of the veneer was 12 mm min⁻¹. The immersion depth was 10 mm and the withdrawing position was 5 mm above the water. To prevent end-grain water penetration and fast longitudinal liquid transportation during measurement, the cross section of the tested wood veneer was coated by polyurethane lacquer before the measurement. Based on the immersion depth and the immersion and withdrawal velocity of the veneer, the wood veneer contacted with the water for a total of ca 167 min during the 100 cycles.

For porous and hygroscopic samples like wood, the measured force F can be written as (Wålinder and Ström 2001):

$$F(h, t) = Py\cos\theta + F_w(t) - \rho Ahg$$
 (2)

where $Py \cos \theta$ equals the wetting force and P is the wetted perimeter of the wood veneer, y the surface tension of the probe liquid, and θ the liquid-solid-air CA; ρ *Ahg* corresponds to the buoyancy force and ρ is the probe liquid density, A the cross-sectional area of the veneer, h the immersion depth, g the gravitational constant and $F_w(t)$ the force due to sorption of the liquid at time t. The advancing angle θ_a and receding angle θ_r at cycle n can be obtained by linear regression of the corresponding curves extrapolated to zero depth (h = 0) in the multicycle Wilhelmy plate plot (cf. Figure 6), assuming that *P* and *y* are constant, and Eq. (2) can be simplified to:

$$F_{ad,n} = P\gamma \cos \theta_{a,n} + F_{f,n-1} \tag{3}$$

$$F_{ad,n} = P\gamma \cos \theta_{a,n} + F_{f,n-1}$$

$$F_{re,n} = P\gamma \cos \theta_{r,n} + F_{f,n}$$
(4

where $F_{f,n-1}$ and $F_{f,n}$ are the final forces after cycle n-1 and n, respectively, which are caused by the sorption. The $F_{f,n-1}$ and $F_{f,n}$ are equal to the term $F_w(t)$ in Eq. (2). The two CAs at cycle n, $\theta_{a,n}$ and $\theta_{r,n}$, can be calculated as:

$$\cos \theta_{a,n} = \frac{F_{a,n} - F_{f,n-1}}{P\gamma}$$

$$\cos \theta_{r,n} = \frac{F_{r,n} - F_{f,n}}{P\gamma}$$
(6)

$$\cos \theta_{r,n} = \frac{F_{r,n} - \dot{F}_{f,n}}{P_V} \tag{6}$$

Sorption is determined by linear regression of the final force, F_{f_2} to zero depth for each cycle.

The liquid uptake of wood veneer after cycle n, W_n is calculated as:

$$W_n = \frac{F_{f,n}}{mg} \times 100\% \tag{7}$$

where m is the initial mass of the wood sample before sealing.

3 Results and discussion

3.1 Silicone nanofilaments preparation conditions

The relative humidity RH in the reaction chamber affects the formation of polysiloxane nano- and microstructures in the gas-phase based reaction. The different preparation conditions lead to the formation of different structures, e.g., nanofilaments, microrods and mixtures of them (Artus et al. 2017). It has been shown that the silicone nanofilaments can form in a rather broad RH range, i.e., between 20 and 60% RH, at room temperature during the synthesis (Artus et al. 2017; Olveira et al. 2018). In this work, liquid water was used in the reaction chamber at reduced pressure. The liquid started evaporating upon reduction of pressure, which was accompanied by the increase of RH in the chamber. This process can produce a high RH in the chamber quickly, thus facilitating the growth of silicone nanofilaments.

As can be seen in Figure 1b, the RH was low at start due to the removal of air in the reaction chamber at reduced pressure. It increased quickly to around 20% RH in a few minutes due to the continuous evaporation of the water, which was suitable for the growth of silicone nanofilaments (Artus and Seeger 2014). The RH reached a plateau of around 40% RH in 30-60 min which was ideal for the synthesis of silicone nanofilaments (Zimmermann et al. 2008).

3.2 Morphology

The surface morphology as seen by SEM and the silicone nanofilaments diameter distribution at the reaction times of 1, 2, 5, and 20 h for SMB and SMAB samples are shown in Figures 2 and 3, respectively. Silicone nanofilaments with

large length-to-diameter ratios were observed on both the SMB and SMAB wood surfaces already at short reaction times (1 and 2 h). These structures were mainly located on the wood cell walls as indicated clearly in Figure 3e. Some micrometer rods with relatively large diameters were observed as well. These microrods, which were mainly located on the wood cell walls and distributed sparsely, were present especially at short reaction times. Most of these structures completed their growth at 2h and were less apparent at longer reaction times. The nanometer filament structures became the dominant structures when the reaction time was increased to 5 h and the coverage of the silicone nanofilaments on the wood surfaces increased accordingly. A dense silicone nanofilamental network was formed on both SMB and SMAB wood surfaces. The sideview SEM image which shows the nanofilaments lying on the wood with a few micrometers in length standing on the surfaces can be found in the previous work (Yin et al. 2020). Due to the heterogeneity of the wood surfaces, however, some areas were not covered with the silicone nanofilaments on both SMB and SMAB, even when the reaction time was increased to 20 h. Since there is no obvious coverage change between 5 and 20 h, we conclude that a reaction time of 5 h is sufficient for good silicone nanofilaments coverage on the wood surfaces when preparing the silicone nanofilaments at reduced pressure.

The average diameter of silicone nanofilaments on both SMB and SMAB followed a similar change, i.e., it decreased with increasing reaction time. The decrease of the diameter is possibly due to the decrease of relative humidity in the reaction chamber with increasing reaction time (Olveira et al. 2018). The differences between 5 and 20 h were, however, small since most of the silicone nanofilaments finished growing after 5 h.

It is usually regarded that the hydroxyl groups on the substrate are responsible for the growth of silicone nanofilaments on the substrate surface (Artus and Seeger 2014). As known, the freely accessible hydroxyl groups in the acetylated wood substance are reduced. There is however no obvious change in silicone nanofilaments distribution on the surfaces comparing SMB and SMAB samples prepared at the same time. This suggests that the decrease in accessible hydroxyl groups in the acetylated wood did not hinder the synthesis of silicone nanofilaments. On the other hand, the silicone nanofilaments with larger average diameters were observed on the SMAB at longer preparation times (5 and 20 h), indicating that the decrease in accessible hydroxyl groups in wood can lead to a growth of the silicone nanofilaments in diameter.

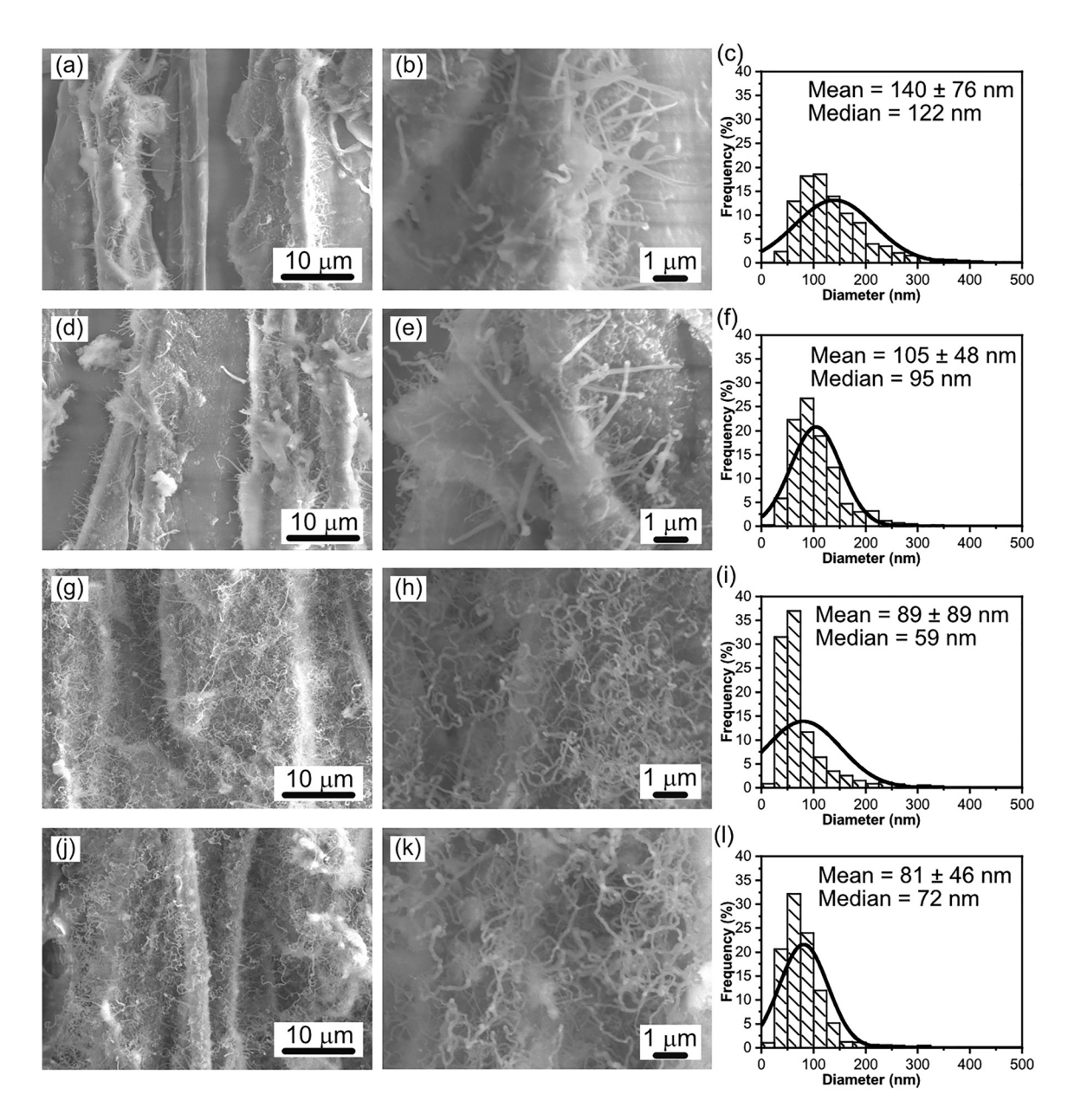


Figure 2: Top-view SEM images of surface-modified birch (SMB) samples and the corresponding number-frequency per 25 nm size class and normal distribution curve (fitted to the data) of the silicone nanofilaments on the surfaces at the reaction time of (a, b, c) 1 h, (d, e, f) 2 h, (g, h, i) 5 h, and (j, k, l) 20 h. The average diameter with standard deviation and the median values of the polysiloxane structures on SMB at different reaction times are given.

3.3 Surface chemistry

The formation of the silicone nanofilaments on the surface-modified wood surfaces is confirmed by FTIR spectra in Figure 4. Since there were only small differences regarding the related absorption peaks, only the FTIR spectra of the surface-modified wood prepared at 5 h are shown. Two absorption peaks at 780 and 1270 cm⁻¹ appeared for SMB and SMAB samples, which

correspond to the stretching vibrations of Si-C bond and -CH3 deformation vibrations of the siloxane compounds, respectively (Cunha et al. 2010; Tang et al. 2016). An additional peak assigned to the C-H bond from Si-CH₃ was observed at 2969 cm⁻¹ on SMB and SMAB. These results confirmed the successful synthesis of polysiloxane on the wood surface.

Apart from the peak changes related to the silicone nanofilaments, an obvious intensity increase was

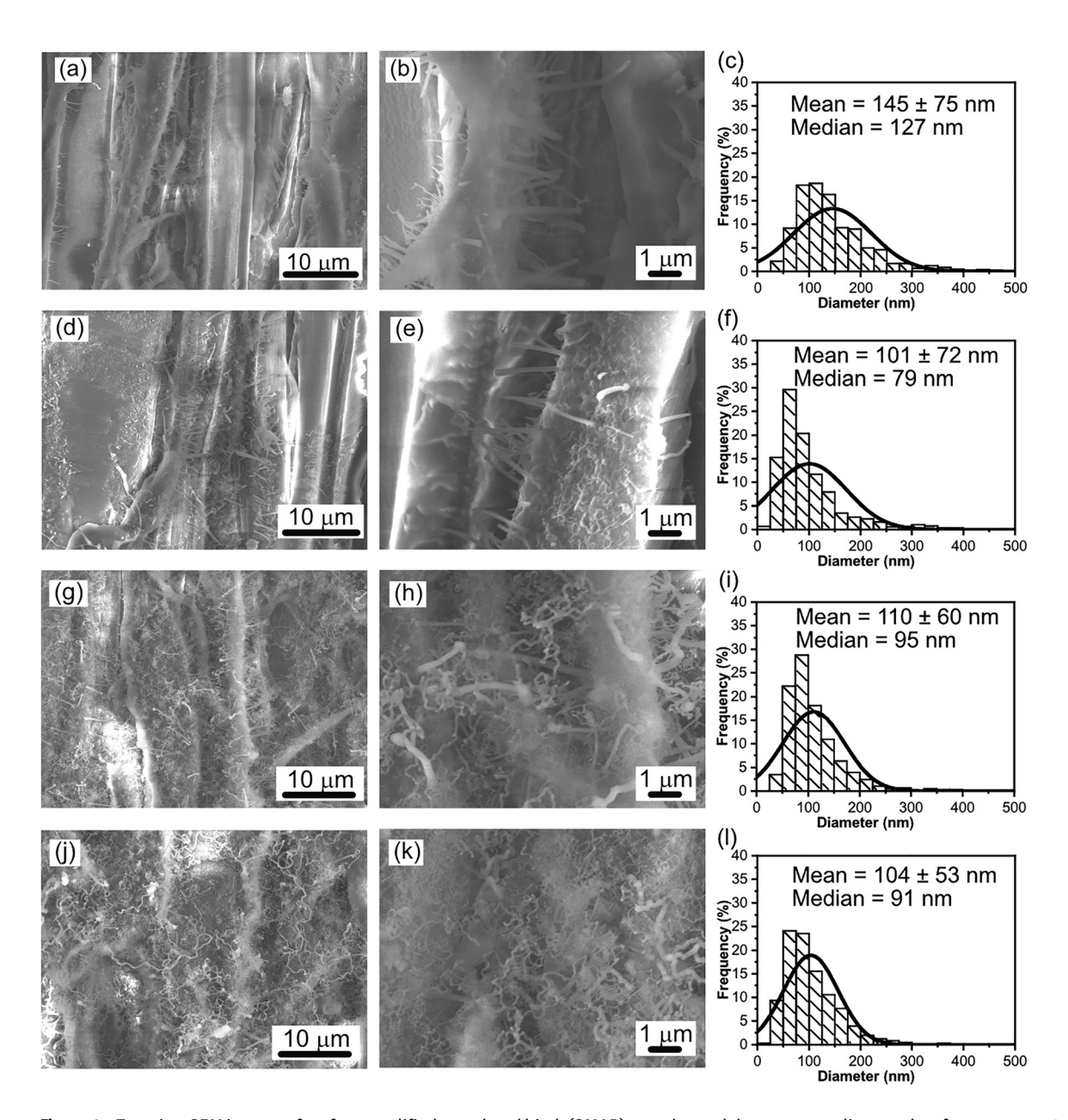


Figure 3: Top-view SEM images of surface-modified acetylated birch (SMAB) samples and the corresponding number-frequency per 25 nm size class and normal distribution curve (fitted to the data) of the silicone nanofilaments on the surfaces at the reaction time of (a, b, c) 1 h, (d, e, f) 2 h, (g, h, i) 5 h, and (j, k, l) 20 h. The average diameter with standard deviation and the median values of the polysiloxane structures on SMAB at different reaction times are given.

observed for the acetylated birch and SMAB samples at the absorption peaks of 1740, 1370, 1220, and 897 cm⁻¹, which were assigned to the stretching of C=O bonds, the deformational vibration of C-H bonds in the methyl group, the stretching of C-O bonds and the vibration of methyl groups, respectively (Mohammed-Ziegler et al. 2008; Pries et al. 2013). Since the acetylated wood could still absorb moisture, the reduction of the broad hydroxyl peak in the region of 3200-3500 cm⁻¹ was less obvious.

3.4 Color change

Figure 5 shows the lightness and color changes of SMB and SMAB wood samples at different reaction times. The original color (OC) and final color (FC) after the surface modification (at silicone nanofilaments reaction time of 1 and 20 h) of the wood samples are shown in Figure 5d. As shown, the color of SMAB wood varied in a small range regarding the three parameters, viz., ΔL^* , Δa^* , and Δb^* . The ΔE^* was smaller than two at all reaction times, suggesting

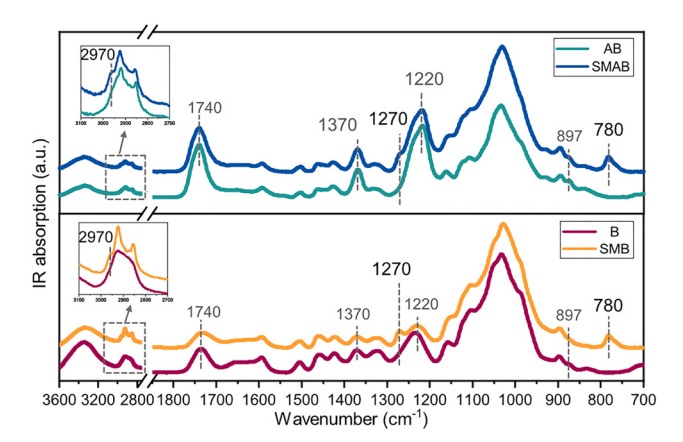


Figure 4: FTIR spectra of the birch (B), acetylated birch (AB), and surface-modified birch (SMB) and surface-modified acetylated birch (SMAB) samples prepared at 5 h. The absorption bands at 2970, 1270, and 780 cm⁻¹ represent silicone nanofilaments and the absorption bands at 1740, 1370, 1220, and 897 cm⁻¹ indicate the acetylation of wood.

that the color change was not detectable by the naked eye (Barcík et al. 2015). On the contrary, the ΔL^* of the SMB wood surface shifted from -1.3 to -7.5 from reaction time 1 to 20 h, which indicates that the surface becomes darker upon increasing reaction time. The Δa^* and Δb^* values also changed with the reaction time, but they were less obvious as the color change values were smaller than three. The ΔE^* increased with increasing reaction time and it was higher

than three already at 2 h. The ΔE^{\star} increased to 8.4 \pm 0.6 at 20 h, suggesting the color change of SMB wood was clearly seen. From the inserted images of the wood samples in Figure 5d, it was obvious that SMB samples showed more color change after surface modification, especially at 20 h. Therefore, the surface modification results in more color change for the non-acetylated wood than for the acetylated wood.

The color change of the wood samples is caused by the release of hydrochloric acid during the surface modification process. Acids can catalyze the condensation and degradation reactions in lignin structures and contribute to the discoloration of wood (Chen et al. 2012; Lundquist 1970; Sundqvist 2004). Since some lignin components in wood are modified in the acetylation process (Rowell et al. 1994), the color change of the acetylated wood in the surface modification is less obvious.

3.5 Wettability

Table 1 gives the CA and ROA of SMB and SMAB samples toward water at different reaction times. It should be mentioned that the results for SMB and SMAB samples can only partially represent the surfaces as only droplets that can be analyzed were considered. Due to the heterogeneity of wood surfaces, some drops rolled off immediately after

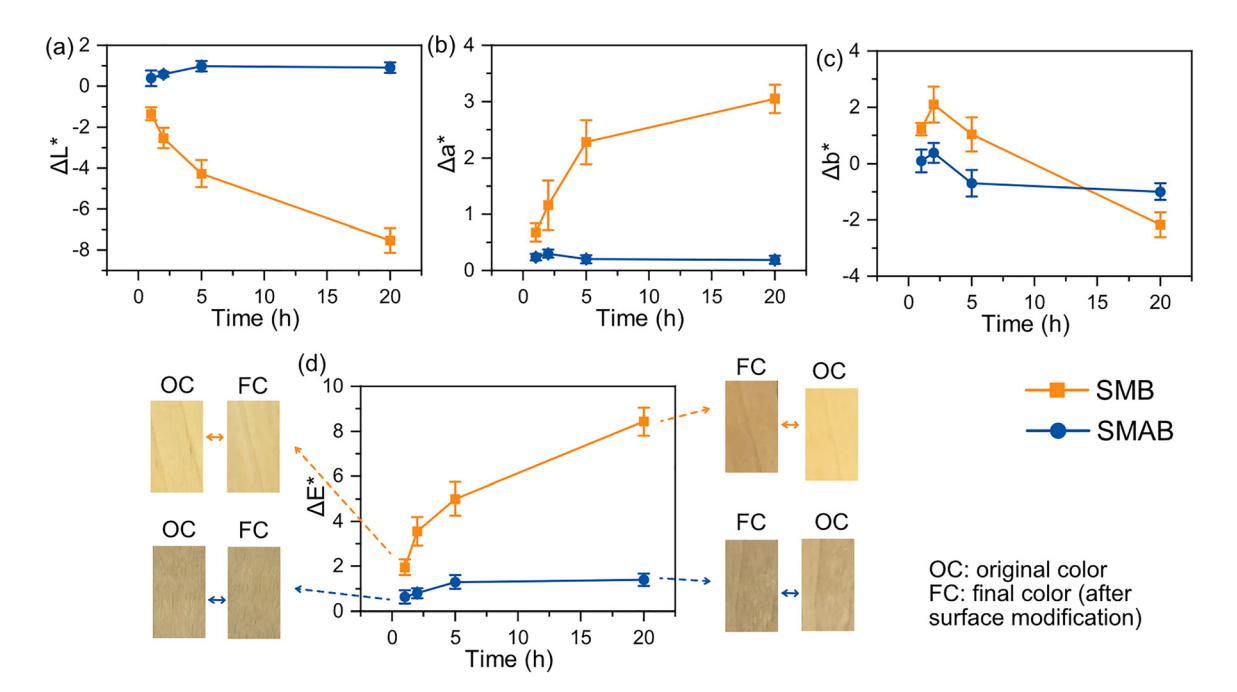


Figure 5: Changes in (a) lightness ΔL^* , (b) redness Δa^* , (c) yellowness Δb^* , and (d) total color change ΔE^* of surface-modified birch (SMB) and surface-modified acetylated birch (SMAB) wood samples after the surface modification at different silicone nanofilaments reaction times. The original color (OC) and final color (FC) of wood samples prepared at 1 and 20 h are given in Figure 5d.

Table 1: Static water contact angles (CAs) and roll-off angles (ROAs) with standard deviations of surface-modified birch (SMB) and surface-modified acetylated birch (SMAB) at different reaction times.^a

| Reaction time (h) | Sample name | CA (°) | ROA (°) | Sample name | CA (°) | ROA (°) |
|-------------------|-------------|-------------|-------------|------------------|-------------|------------|
| 1 | SMB | 164 ± 6 | 34 ± 20 | SMAB | 163 ± 5 | 26 ± 19 |
| 2 | | 162 ± 5 | 44 ± 17 | | 162 ± 4 | 26 ± 7 |
| 5 | | 163 ± 6 | 26 ± 16 | | 164 ± 4 | 14 ± 5 |
| 20 Birch | | 163 ± 3 | 42 | | 163 ± 5 | 11 ± 10 |
| | Birch | 59 ± 7 | n/a | Acetylated birch | 64 ± 8 | n/a |

^aDue to the heterogeneity of wood surfaces, some drops rolled off immediately after dispensing while some other drops pinned on the surfaces. The static contact angles were calculated based on the drops that did not roll off immediately after dispensing and the roll-off angles were calculated based on the drops that did not roll off immediately but rolled off at certain degrees. The specific information: i) 1 h, one of 13 of the dispensed drops rolled off immediately while two of 13 of the dispensed drops pinned on the SMB surfaces; one of 11 of the dispensed drops rolled off immediately while three of 11 of the dispensed drops pinned on the SMAB surfaces; iii) 2 h, nine of 13 of the dispensed drops pinned on the SMB surfaces; all dispensed drops rolled off immediately while one of 16 of the dispensed drops pinned on the SMB surfaces; all dispensed drops rolled off at certain degrees on the SMAB surfaces; iv) 20 h, only one dispensed drop rolled off on the SMB surfaces; one of seven of the dispensed drops rolled off immediately while no dispensed drops pinned on the SMAB surfaces.

dispensing while some other drops pinned on the surfaces. As shown in Table 1, the birch and acetylated birch wood showed a CA of 59 \pm 7° and 64 \pm 8°, respectively. The silicone nanofilaments coating increased the static CA significantly, resulting in a CA of 164 \pm 6° and 163 \pm 5°, respectively, for the SMB and SMAB samples prepared at 1 h. The silicone nanofilaments coating did not show an obvious difference between SMB and SMAB regarding the static CAs. Values varying from 162° to 164° were observed for both the SMB and SMAB samples prepared at longer times, indicating the reaction time did not affect the static CAs too much. On the other hand, the ROA of the SMAB sample decreased from $26 \pm 19^{\circ}$ at 1 h to $11 \pm 10^{\circ}$ at 20 h, suggesting that the reaction time can improve the water repellence of the acetylated wood surfaces. However, this decreasing trend was not observed for the SMB sample. Given the fact that wood is heterogeneous and the surfacemodified wood samples show high static CA and low ROA for the longer reaction time, it is concluded that the modified wood is superhydrophobic. Moreover, the modified wood surfaces maintained the water repellence even after a few cycles of tape peeling test as shown in the Supplementary Video (Movie S1, SMB prepared at 20 h), suggesting that the stability of the silicone nanofilaments layer was good.

The sessile drop measurement is more useful for measuring the wetting property of a smooth and homogeneous surface. As known, the wood is hygroscopic and swellable and its surfaces are heterogeneous, which makes the wetting process complex especially when using a polar liquid. In the study of the wettability of the SMB and SMAB, the static CAs and roll-off angles can only represent the specific spots as the surface-modified wood samples are

still heterogeneous. The Wilhelmy plate method is regarded as a more accurate method for evaluating the wetting property of wood as a large area can be covered during the measurement and an average value is obtained which enables a high reproducibility. The multicycle Wilhelmy plate measurement allows the study of the dynamic wetting and dewetting of the superhydrophobic wood, as well. Furthermore, the liquid uptake of wood can be achieved in the repeated immersion cycles.

Figure 6 shows results from the 100-cycle Wilhelmy plate measurements for selected birch, acetylated birch, as well as SMB and SMAB samples. The birch and acetylated birch showed an initial θ_a of 93° and 75°, respectively. However, the $\theta_{\rm r}$ value in all cycles and the $\theta_{\rm a}$ in all subsequent cycles were zero, suggesting the wood surfaces were completely wetted in water in the absence of surface modification. The force detected after the removal of the sample from the liquid increased with increasing immersion cycle and this was caused by water sorption. The SMB and SMAB showed an initial $\theta_{a,1}$ of 124° and 146°, and an initial $\theta_{r,1}$ of 82° and 90°, respectively, indicating the water repellence of the wood surfaces was effectively improved by the silicone nanofilaments. Moreover, only a small increase in the detected force was observed for both SMB and SMAB when removing the sample from water after 100 cycles.

Table 2 summarizes the θ_a , θ_r and contact angle hysteresis (CAH) for the SMB and SMAB at specific cycles. The θ_a and θ_r show a decreasing trend with increasing cycles and the largest drop was observed in the first 10 cycles for both the SMB and SMAB samples. Furthermore, the SMAB showed higher θ_a s and θ_r s than those of the SMB. Meanwhile, it showed lower CAHs. Therefore, the SMAB shows a greater liquid repellence than the SMB.

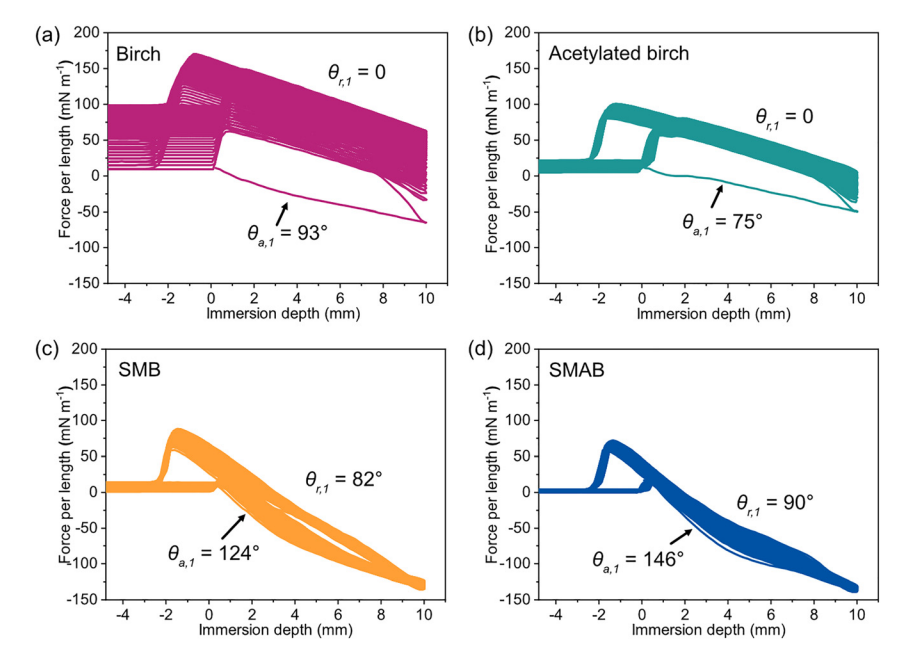


Figure 6: Force per perimeter length as a function of sample position for 100-cycle Wilhelmy plate measurements for (a) birch, (b) acetylated birch, (c) surface-modified birch (SMB), and (d) surface-modified acetylated birch (SMAB) prepared at 5 h.

Table 2: Advancing angle θ_a and receding angle θ_r and contact angle hysteresis CAH with standard deviations for surface-modified birch (SMB) and surface-modified acetylated birch (SMB) samples prepared at 5 h at specific cycles.

| Cycle no. | SMB | | | SMAB | | |
|-----------|------------------------|---------------------------|------------|--------------------|--------------------------|-------------|
| | $\theta_{a}(^{\circ})$ | θ _r (°) | CAH (°) | θ _a (°) | $	heta_{ m r}(^{\circ})$ | CAH (°) |
| 1 | 122 ± 3 | 70 ± 11 | 52 ± 11 | 154 ± 8 | 89 ± 7 | 65 ± 9 |
| 10 | 93 ± 23 | 48 ± 22 | 45 ± 6 | 109 ± 12 | 72 ± 16 | 38 ± 14 |
| 50 | 89 ± 27 | 36 ± 32 | 53 ± 5 | 90 ± 17 | 67 ± 21 | 23 ± 4 |
| 100 | 87 ± 27 | 37 ± 33 | 51 ± 6 | 85 ± 15 | 63 ± 22 | 22 ± 7 |

Figure 7 shows the water uptake versus the immersion cycle obtained from the 100-cycle Wilhelmy curves. The water uptake of unmodified birch increased dramatically with the increasing immersion cycles, approaching 86 ± 6 wt% after 100 cycles. The acetylated birch showed a much lower water uptake rate, leading to final water uptake of 15 \pm 3 wt%, almost six times lower than that of the birch wood. The SMB exhibited an even slower water uptake behavior as a result of the superhydrophobic coating, ending at 10 ± 1 wt% after 100 cycles, which was 8.6 and 1.5 times lower than that of the birch and acetylated birch, respectively. This result suggests that the surface modification of wood by silicone nanofilaments shows more pronounced improvement regarding the water-resistance property of wood than the acetylation of wood. The water uptake of SMAB was as low as 3 ± 1 wt% after 100 cycles, which was about 29, 5, and 3 times lower than that of the birch, acetylated birch and SMB, respectively. To conclude, remarkably reduced water uptake of wood was obtained by

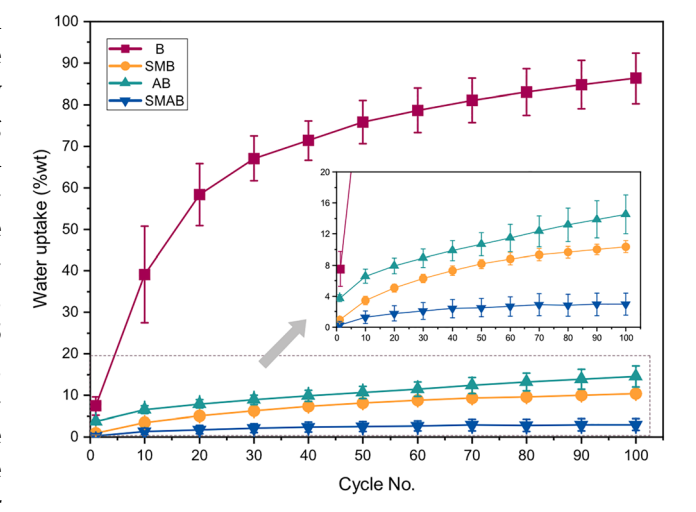


Figure 7: Water uptake from multi-cycle Wilhelmy measurements with standard deviation as a function of cycle number for birch (B), acetylated birch (AB) and surface-modified birch (SMB) and surface-modified acetylated birch (SMAB) samples prepared at 5 h.

combining the acetylated wood with the superhydrophobic coating.

Unmodified wood is hygroscopic due to its porous structure and the hydrophilic nature of its components. The liquid sorption process for the unmodified wood includes the wetting of the surfaces, the gradually filling of the wood voids through capillaries and the continuous diffusion and swelling in the wood structures (Sedighi Moghaddam et al. 2014). As a result, the water uptake of the unmodified wood can be high after long-time contact with water. For acetylated wood, the wood affinity for water is reduced mainly due to the reduction of primary sorption sites and the decrease of the volume in the wood cell walls which is available to water (Popescu et al. 2013; Rowell 2014). But the acetylated birch wood is still hydrophilic and the porosity of the wood is not changed. Therefore, the water can still be absorbed into the porous structures in wood. It was reported the acetylation mainly reduced the liquid uptake by reducing the swelling (Sedighi Moghaddam et al. 2016b). For the surface-modified non-acetylated wood, the superhydrophobic coating layer acts as a barrier, effectively repelling the water from the wood surfaces. Due to the diffusion effect, SMB wood can still absorb water. In addition, solubility in the nanofilaments layer for water can contribute to the liquid penetration, as suggested (Yin et al. 2020). The wood affinity for water inside the porous wood structures is not changed compared to the unmodified wood. Therefore, the water uptake of the SMB increased gradually upon long-time contact with water. In the 100-cycle Wilhelmy measurement, the SMB wood showed lower water uptake than the acetylated birch wood, suggesting that the silicone nanofilaments coating is more efficient in repelling water than the acetylation. For the surface-modified acetylated wood, on the one hand, it is able to repel water from the surfaces due to the superhydrophobic silicone nanofilaments layer; on the other hand, it shows low affinity for water sorption owing to the acetylation. Therefore, extremely low water uptake was obtained for the SMAB wood.

As known, the acetylated wood shows good resistance against fungi and mechanical properties, and superhydrophobic surfaces generally show good self-cleaning properties. These aspects were not investigated in this study, but it is believed that the surface-modified acetylated wood can also bring such functional properties to the wood.

4 Conclusions

The applied non-fluorine surface modification, even at shorter reaction times, results in static water contact angles greater than 160° and low roll-off angles on both the birch and the acetylated birch samples, i.e., a superhydrophobic behavior. Dynamic wettability was studied by a multicycle Wilhelmy plate method, which showed a remarkably low water uptake of the surface-modified acetylated samples in the repeated wetting cycles in water, about 29 and 5 times lower than that of the non-surface-modified birch and acetylated birch, respectively. Moreover, the water uptake of the surface-modified acetylated birch samples was three times lower than that of the surface-modified birch. The low water uptake of surface-modified acetylated wood is caused by a combined effect of high water repellence of the surface and the low affinity for water sorption of the acetylated (bulk-modified) cell-wall. In addition, the applied surface modification brings only small color changes on the wood surfaces, especially for the acetylated samples.

Author contributions: All the authors have accepted responsibility for the entire content of this submitted manuscript and approved submission.

Research funding: Formas research council acknowledged for funding the project "Durable water-, oil- and soil repellent wood for outdoor applications via smart surface modification", grant no. 2016-01362. The Vinnova project 2017-02712 "Bärande utomhusträ" within the BioInnovation program is also acknowledged for supporting the project.

Conflict of interest statement: The authors declare no conflicts of interest regarding this article.

References

ACCSYS. (2020). What is acetylation? How we enhance nature, Available at: https://www.accsysplc.com/products/what-isacetylation/ (Accessed 28 September 2020).

Artus, G.R., Olveira, S., Patra, D., and Seeger, S. (2017). Directed in situ shaping of complex nano- and microstructures during chemical synthesis. Macromol. Rapid Commun. 38: 1600558.

Artus, G.R., and Seeger, S. (2014). One-dimensional silicone nanofilaments. Adv. Colloid Interface Sci. 209: 144-162.

Barcík, S., Gašparík, M., and Razumov, E.Y. (2015). Effect of temperature on the color changes of wood during thermal modification. Cellul. Chem. Technol. 49: 789-798.

- Beck, G., Thybring, E.E., and Thygesen, L.G. (2018). Brown-rot fungal degradation and de-acetylation of acetylated wood. Int. Biodeterior. Biodegrad. 135: 62-70.
- Bongers, F., and Uphill, S. (2019). Performance of acetylated wood in aquatic applications. Int. Wood Prod. J. 10: 95-101.
- Bryne, L.E., and Wålinder, M.E. (2010). Ageing of modified wood. Part 1: wetting properties of acetylated, furfurylated, and thermally modified wood. Holzforschung 64: 295-304.
- Cademartori, P.H.G.D., Stafford, L., Blanchet, P., Magalhães, W.L.E., and Muniz, G.I.B.D. (2017). Enhancing the water repellency of wood surfaces by atmospheric pressure cold plasma deposition of fluorocarbon film. RSC Adv. 7: 29159-29169.
- Chai, Y., Liu, J., Wang, Z., and Zhao, Y. (2017). Dimensional stability and mechanical properties of plantation poplar wood esterified using acetic anhydride. Bioresources 12: 912-922.
- Chen, Y., Fan, Y., Gao, J., and Stark, N.M. (2012). The effect of heat treatment on the chemical and color change of black locust (Robinia pseudoacacia) wood flour. Bioresources 7: 1157-1170.
- Cunha, A.G., Freire, C., Silvestre, A., Pascoal Neto, C., Gandini, A., Belgacem, M.N., Chaussy, D., and Beneventi, D. (2010). Preparation of highly hydrophobic and lipophobic cellulose fibers by a straightforward gas-solid reaction. J. Colloid Interface Sci. 344: 588-595.
- Gao, L., Lu, Y., Zhan, X., Li, J., and Sun, Q. (2015). A robust, anti-acid, and high-temperature-humidity-resistant superhydrophobic surface of wood based on a modified TiO2 film by fluoroalkyl silane. Surf. Coating. Technol. 262: 33-39.
- Guo, H., Fuchs, P., Casdorff, K., Michen, B., Chanana, M., Hagendorfer, H., Romanyuk, Y.E., and Burgert, I. (2017). Bio-inspired superhydrophobic and omniphobic wood surfaces. Adv. Mater. Interfac. 4: 1600289.
- Hansmann, C., Schwanninger, M., Stefke, B., Hinterstoisser, B., and Gindl, W. (2004). UV-microscopic analysis of acetylated spruce and birch cell walls. Holzforschung 58: 483-488.
- Herrera, R., Arrese, A., de Hoyos-Martinez, P.L., Labidi, J., and Llano-Ponte, R. (2018). Evolution of thermally modified wood properties exposed to natural and artificial weathering and its potential as an element for façades systems. Construct. Build. Mater. 172: 233-242.
- Hill, C.A. (2006). Wood modification: chemical, thermal and other processes. John Wiley & Sons, Chichester.
- Hung, K.-C., Wu, T.-L., Chen, Y.-L., and Wu, J.-H. (2016). Assessing the effect of wood acetylation on mechanical properties and extended creep behavior of wood/recycled-polypropylene composites. Construct. Build. Mater. 108: 139-145.
- Joffre, T., Segerholm, K., Persson, C., Bardage, S.L., Hendriks, C.L.L., and Isaksson, P. (2017). Characterization of interfacial stress transfer ability in acetylation-treated wood fibre composites using X-ray microtomography. Ind. Crop. Prod. 95: 43-49.
- Källbom, S., Moghaddam, M.S., and Wålinder, M.E. (2018). Liquid sorption, swelling and surface energy properties of unmodified and thermally modified Scots pine heartwood after extraction. Holzforschung 72: 251-258.
- Källbom, S., Lillqvist, K., Spoljaric, S., Seppälä, J., Segerholm, K., Rautkari, L., Hughes, M., and Wålinder, M. (2020). Effects of water soaking-drying cycles on thermally modified spruce wood-plastic composites. Wood Fiber Sci. 52: 2-12.
- Laine, K., Segerholm, K., Wålinder, M., Rautkari, L., Hughes, M., and Lankveld, C. (2016). Surface densification of acetylated wood. Eur. J. Wood Prod. 74: 829-835.

- Lundquist, K. (1970). Acid degradation of lignin. Acta Chem. Scand. 24: 889-907.
- Meyer-Veltrup, L., Brischke, C., Alfredsen, G., Humar, M., Flæte, P.-O., Isaksson, T., Brelid, P.L., Westin, M., and Jermer, J. (2017). The combined effect of wetting ability and durability on outdoor performance of wood: development and verification of a new prediction approach. Wood Sci. Technol. 51: 615-637.
- Mohammed-Ziegler, I., Tánczos, I., Hórvölgyi, Z., and Agoston, B. (2008). Water-repellent acylated and silylated wood samples and their surface analytical characterization. Colloid. Surface. Physicochem. Eng. Aspect. 319: 204-212.
- Olveira, S., Stojanovic, A., and Seeger, S. (2018). Systematic parametric investigation on the CVD process of polysiloxane nano-and microstructures. J. Nanoparticle Res. 20: 307.
- Pandit, S.K., Tudu, B.K., Mishra, I.M., and Kumar, A. (2020). Development of stain resistant, superhydrophobic and self-cleaning coating on wood surface. Prog. Org. Coating 139: 105453.
- Popescu, C.-M., Hill, C.A.S., Curling, S., Ormondroyd, G., and Xie, Y. (2013). The water vapour sorption behaviour of acetylated birch wood: how acetylation affects the sorption isotherm and accessible hydroxyl content. J. Mater. Sci. 49: 2362-2371.
- Pries, M., Wagner, R., Kaesler, K.-H., Militz, H., and Mai, C. (2013). Acetylation of wood in combination with polysiloxanes to improve water-related and mechanical properties of wood. Wood Sci. Technol. 47: 685-699.
- Ringman, R., Pilgård, A., and Richter, K. (2020). Brown rot gene expression and regulation in acetylated and furfurylated wood: a complex picture. Holzforschung 74: 391-399.
- Rowell, R. (2007). Chapter 22. Chemical modification of wood. In: Handbook of engineering biopolymers-homopolymers, blends and composites. Hanser Publishers, Munchen, pp. 673-691.
- Rowell, R. (2014). Acetylation of wood a review. Int. J. Lignocellulosic Prod. 1: 1-27.
- Rowell, R.M., Simonson, R., Hess, S., Plackett, D.V., Cronshaw, D., and Dunningham, E. (1994). Acetyl distribution in acetylated whole wood and reactivity of isolated wood cell-wall components to acetic anhydride. Wood Fiber Sci. 26: 11-18.
- Sedighi Moghaddam, M., Walinder, M.E., Claesson, P.M., and Swerin, A. (2013). Multicycle Wilhelmy plate method for wetting properties, swelling and liquid sorption of wood. Langmuir 29: 12145-53.
- Sedighi Moghaddam, M., Claesson, P.M., Wålinder, M.E.P., and Swerin, A. (2014). Wettability and liquid sorption of wood investigated by Wilhelmy plate method. Wood Sci. Technol. 48: 161-176.
- Sedighi Moghaddam, M., Heydari, G., Tuominen, M., Fielden, M., Haapanen, J., Mäkelä, J.M., Wålinder, M.E.P., Claesson, P.M., and Swerin, A. (2016a). Hydrophobisation of wood surfaces by combining liquid flame spray (LFS) and plasma treatment: dynamic wetting properties. Holzforschung 70: 527-537.
- Sedighi Moghaddam, M., Wålinder, M.E.P., Claesson, P.M., and Swerin, A. (2016b). Wettability and swelling of acetylated and furfurylated wood analyzed by multicycle Wilhelmy plate method. Holzforschung 70: 69-77.
- Sundavist, B. (2004). Colour changes and acid formation in wood during heating, Doctoral thesis. Skellefteå Campus, Luleå tekniska universitet.
- Swerin, A. and Wåhlander, M. (2009). On fundamentals and applications of superhydrophobicity in papermaking and packaging. In: XIVth fundamental research symposium, advances in pulp and paper research. Fundamental Research Committee, Stockholm.

- Tang, Z., Xie, L., Hess, D.W., and Breedveld, V. (2016). Fabrication of amphiphobic softwood and hardwood by treatment with nonfluorinated chemicals. Wood Sci. Technol. 51: 97-113.
- Teisala, H., and Butt, H.J. (2018). Hierarchical structures for superhydrophobic and superoleophobic surfaces. Langmuir 35: 10689-10703.
- Tuominen, M., Teisala, H., Haapanen, J., Mäkelä, J.M., Honkanen, M., Vippola, M., Bardage, S., Wålinder, M.E.P., and Swerin, A. (2016). Superamphiphobic overhang structured coating on a biobased material. Appl. Surf. Sci. 389: 135-143.
- Tuteja, A., Choi, W., McKinley, G.H., Cohen, R.E., and Rubner, M.F. (2011). Design parameters for superhydrophobicity and superoleophobicity. MRS Bull. 33: 752-758.
- Wålinder, M.E., and Ström, G. (2001). Measurement of wood wettability by the Wilhelmy method. Part 2. Determination of apparent contact angles. Holzforschung 55: 33-41.

- Wang, Y., Tang, Z., Lu, S., Zhang, M., Liu, K., Xiao, H., Huang, L., Chen, L., Wu, H., and Ni, Y. (2020). Superhydrophobic wood grafted by poly(2-(perfluorooctyl)ethyl methacrylate) via ATRP with selfcleaning, abrasion resistance and anti-mold properties. Holzforschung 74: 799-809.
- Yin, H., Sedighi Moghaddam, M., Tuominen, M., Eriksson, M., Järn, M., Dėdinaitė, A., Wålinder, M., and Swerin, A. (2020). Superamphiphobic plastrons on wood and their effects on liquid repellence. Mater. Des. 195: 108974.
- Zimmermann, J., Reifler, F.A., Fortunato, G., Gerhardt, L.-C., and Seeger, S. (2008). A simple, one-step approach to durable and robust superhydrophobic textiles. Adv. Funct. Mater. 18: 3662-3669.

Supplementary Material: The online version of this article offers supplementary material (https://doi.org/10.1515/hf-2020-0236).